Brownian Coagulation at High Concentration

M. C. Heine and S. E. Pratsinis*

Particle Technology Laboratory, Institute of Process Engineering, Department of Mechanical and Process Engineering, ETH Zurich, 8092 Zürich, Switzerland

Received April 30, 2007. In Final Form: June 12, 2007

Particle growth by Brownian coagulation at high concentration in the continuum regime is investigated by solving the Langevin dynamics (LD) equations for each particle trajectory of polydisperse suspensions. By monitoring the LD attainment of the self-preserving size distribution (SPSD), it is shown that the classic Smoluchowski collision frequency function is accurate for dilute particle volume fractions, ϕ_s, below 0.1%. At higher ϕ_s, coagulation is about 4 and 10 times faster than for the classic theory at $\phi_s = 10$ and 20%, respectively. For complete particle coalescence upon collision, SPSDs develop even in highly concentrated suspensions (up to $\phi_s = 35\%$), as with dilute ones, but are broadened with increasing ϕ_s. At high particle concentration, an overall coagulation rate is proposed that reduces to the classic one at low concentration. Detailed collision frequency functions are also obtained at various ϕ_s values. Fractal-like agglomerates undergoing coagulation at constant fractal dimension attain an SPSD only temporarily because their effective volume fraction continuously increases, approaching gelation in the absence of restructuring or fragmentation.

1. Introduction

For nearly a century, the classic Smoluchowski equation has been used to describe Brownian coagulation[1] in colloids,[2] emulsions,[3] flocculation,[4] granulation,[5] air pollution,[6] materials manufacture,[7] and soot formation[8] to name a few of its widespread applications. Corrections to that equation have been developed for van der Waals forces, charged or nonspherical particles,[9] electric or magnetic fields,[10] and hydrodynamic particle interactions[11] without altering its basic theoretical framework: the establishment of a steady-state Fickian flux to the particle surface.

That way, the Smoluchowski equation cannot describe the coagulation of highly concentrated colloidal or aerosol suspensions (particle volume fraction above 1%). Such highly concentrated suspensions are well known in emulsions, where the droplet volume fraction may vary from zero to almost one[12] but can also be observed in aerosols. For example, a transition from dilute to concentrated particle dynamics may take place during flame aerosol synthesis of nanostructured, fractal-like carbon black, fumed silica,[13] or titania[14] particles at industrially relevant conditions. Even though in such processes the particle volume fraction, ϕ_s, is only 0.001 to 0.01%, depending on the process temperature, fractal-like silica agglomerates form and grow to occupy more than 10% of the gas volume during typical reactor residence times in the absence of restructuring or fragmentation.[13] Under these conditions, the basic assumption of the Smoluchowski equation, a quasi-steady-state concentration profile around colliding particles, does not hold, as has been pointed out by Smoluchowski[1,13] with respect to employing Fick's laws to the calculation of particle collision frequency. As a result, alternative computational schemes are needed to calculate the coagulation rate of concentrated particulate suspensions.

Direct numerical simulation of particle trajectories by Langevin dynamics (LD) has been used to compute particle motion regardless of concentration. Gutsch et al.[15] investigated the detailed structure evolution of aerosol particles formed by monomer−cluster aggregation by LD simulations. Trzeciak et al.[16] used LD to study the collision frequency function of monodisperse aerosol particles in the Brownian free molecular and continuum regimes and found faster coagulation rates for particles larger than the free mean path of the fluid at $\phi_s > 1\%$. Similarly, Sorensen et al.[17] showed experimentally that soot clusters at high concentrations close to aerogelation grow faster than predicted by classic coagulation theory.

Here, the growth of spherical (complete coalescence upon collision) and fractal-like particles by Brownian coagulation is investigated in the continuum regime by computing the stochastic particle trajectories by the Langevin differential equation. The continuum regime is selected because rather large agglomerates are formed in aerosol reactors when the effective particle volume fraction has grown to high levels.[13] Such LD calculations are compared to those of detailed, highly accurate, sectional population balance models.[18] Particle growth kinetics and size evolution are studied as a function of particle volume fraction for $\phi_s = 0.01-35$ vol %. Emphasis is placed on the attainment of self-preserving size distributions (SPSD) because they greatly facilitate coagulation calculations coupled to fluid mechanics in

* Corresponding author. E-mail: pratsinis@ptl.mavt.ethz.ch. Tel: +41-44-632-3180. Fax: +41-44-632-1595.

(1) Smoluchowski, M. *Z. Phys. Chem.* **1916**, *17*, 557−571 and 585−599.
(2) Broide, M. L.; Cohen, R. J. *J. Colloid Interface Sci.* **1992**, *153*, 493−508.
(3) Urbina-Villalba, G.; Garcia-Sucre, M. *Langmuir* **2000**, *16*, 7975−7985.
(4) Bushell, G. C.; Yan, Y. D.; Woodfield, D.; Raper, J.; Amal, R. *Adv. Colloid Interface Sci.* **2002**, *95*, 1−50.
(5) Iveson, S. M.; Litster, J. D.; Hapgood, K.; Ennis, B. J. *Powder Technol.* **2001**, *117*, 3−39.
(6) Zhang, Y.; Seigneur, C.; Seinfeld, J. H.; Jacobson, M. Z.; Binkowski, F. S. *Aerosol Sci. Technol.* **1999**, *31*, 487−514.
(7) Johannessen, T.; Pratsinis, S. E.; Livbjerg, H. *Chem. Eng. Sci.* **2000**, *55*, 177−191.
(8) Frenklach, M. *Chem. Eng. Sci.* **2002**, *57*, 2229−2239.
(9) Friedlander, S. K. *Smoke, Dust, and Haze: Fundamentals of Aerosol Dynamics*, 2nd ed.; Oxford University Press: New York, 2000.
(10) Tsouris, C.; Scott, T. C. *J. Colloid Interface Sci.* **1995**, *171*, 319−330.
(11) Melis, S.; Verduyn, M.; Storti, G.; Morbidelli, M.; Baldyga, J. *AIChE J.* **1999**, *45*, 1383−1393.
(12) Bibette, J.; Calderon, F. L.; Poulin, P. *Rep. Prog. Phys.* **1999**, *62*, 969−1033.
(13) Heine, M. C.; Pratsinis, S. E. *Langmuir* **2006**, *22*, 10238−10245.
(14) Heine, M. C.; Pratsinis, S. E. *Part. Part. Syst. Charact.* **2007**, *24*, 56−65.
(15) Gutsch, A.; Pratsinis, S. E.; Loffler, F. *J. Aerosol. Sci.* **1995**, *26*, 187−199.
(16) Trzeciak, T. M.; Podgorski, A.; Marijnissen, J. C. M. *Inz. Chem. Procesowa* **2004**, *25*, 1741−1746.
(17) Sorensen, C. M.; Hageman, B.; Rush, T. J.; Huang, H.; Oh, C. *Phys. Rev. Lett.* **1998**, *80*, 1782−1785.
(18) Litster, J. D.; Smit, D. J.; Hounslow, M. J. *AIChE J.* **1995**, *41*, 591−603.

10.1021/la7012599 CCC: $37.00
Published on Web 08/09/2007

industrial particulate processes.[7] Overall coagulation rates at high ϕ_s are obtained that reduce to classic ones at low ϕ_s and approach gelation at high ϕ_s. The dynamics of coagulating fractal-like particles at high concentration is also explored as their effective particle volume fraction continuously increases, approaching gelation.

2. Theory

2.1. Langevin Dynamics. *2.1.1. Particle Trajectories.* Single-particle trajectories can be described by the Langevin differential equation[19]

$$m\dot{\mathbf{v}} = -f(\mathbf{v} - \mathbf{w}) + \sum \mathbf{F}_{\text{ext}} + \sum \mathbf{F}_{i,j} + \mathbf{F}_{\text{B}} \qquad (1)$$

where m and f are the particle mass and friction coefficient and **v** and **w** are particle and fluid velocity vectors, respectively. The first four terms from left to right are identical to those in Newton's equation of motion, namely, the particle acceleration, frictional (drag) force, and the sum of external and interparticle forces. The last term describes the stochastic, rapidly fluctuating force on the particles from the bombardment of fluid molecules. Neglecting external and interparticle forces, partial integration of eq 1 results in[20]

$$\mathbf{v}(t + \Delta t) = \mathbf{V} + \mathbf{v}(t)\mathrm{e}^{-\alpha\Delta t} \qquad (2)$$

$$\mathbf{r}(t + \Delta t) = \mathbf{R} + \mathbf{r}(t) + \frac{\mathbf{v}(t)}{\alpha}(1 - \mathrm{e}^{-\alpha\Delta t}) \qquad (3)$$

where **r** is the particle position. The mass-related friction coefficient α is given by

$$\alpha = \frac{f}{m} = \frac{18\mu}{\rho_{\text{p}} d^2} \quad \text{with} \quad f = 3\pi\mu d \qquad (4)$$

where μ, ρ_{p}, and d are the fluid viscosity, particle density, and diameter, respectively. In eqs 5 and 6, vectors **V** and **R** represent the stochastic components of particle velocity and displacement, respectively:[15,20]

$$\mathbf{V} = \begin{pmatrix} V_x \\ V_y \\ V_z \end{pmatrix} = \sqrt{G}\begin{pmatrix} Y_1 \\ Y_2 \\ Y_3 \end{pmatrix} \qquad (5)$$

and

$$\mathbf{R} = \begin{pmatrix} R_x \\ R_y \\ R_z \end{pmatrix} = \frac{H}{\sqrt{G}}\begin{pmatrix} Y_1 \\ Y_2 \\ Y_3 \end{pmatrix} + \sqrt{I - \frac{H^2}{G}}\begin{pmatrix} Y_4 \\ Y_5 \\ Y_6 \end{pmatrix} \qquad (6)$$

Here, Y_1−Y_6 represent Gaussian-distributed independent random numbers with zero mean and a variance of unity.[21] In the above equations, G and I represent the mean square values of **V** and **R**, respectively, and H describes the average scalar product of **V** and **R**:

$$\begin{pmatrix} G \\ H \\ I \end{pmatrix} = \begin{pmatrix} \sigma_{\text{V}}^2 \\ \sigma_{\text{VR}} \\ \sigma_{\text{R}}^2 \end{pmatrix} = \frac{k_{\text{B}}T}{m}\begin{pmatrix} 1 - \mathrm{e}^{-2\alpha\Delta t} \\ \alpha^{-1}(1 - \mathrm{e}^{-\alpha\Delta t})^2 \\ \alpha^{-2}(2\alpha\Delta t - 3 + 4\mathrm{e}^{-\alpha\Delta t} - \mathrm{e}^{-2\alpha\Delta t}) \end{pmatrix} \qquad (7)$$

2.1.2. Particle Growth. Particle growth is investigated in a fluid at constant temperature that is represented by an initially cubic domain with periodic boundary conditions in all spatial directions (Figure 1). This domain contains a time-dependent number of particles, n, but constant particle volume fraction, ϕ_s,

$$\phi_s = \frac{\pi \sum_{i=1}^{n} d_i^3}{6L_xL_yL_z} \qquad (8)$$

where L_x, L_y, and L_z are the domain dimensions (Figure 1).

Brownian trajectories of particles are calculated by explicit numerical integration of eqs 2 and 3, neglecting van der Waals and electric forces[22] and hydrodynamic interactions[15] as in the classic theory for Brownian coagulation by Smoluchowski.[23] The collision of particles and complete coalescence ($D_{\text{f}} = 3$) take place once two (or multiple) particles (or periodic particle images) touch or overlap (Figure 1). These particles are replaced by a new particle having the combined mass, mass-averaged position, and velocity (momentum balance) of the colliding particles. As a result, particle growth leads to a continuous increase in particle size but a decrease in particle number concentration. The total number of particles, n, is maintained between n_0 and $n_{\text{min}} = 0.5n_0$ by doubling the fluid (domain) volume, $V_{\text{f}} = L_xL_yL_z$, in turn in the x, y, and z directions once n drops to n_{min}. Particles in the new fluid volume are initialized as a periodic image of the particle population of the original domain as dictated by the boundary conditions (Figure 1).

This method is also applied to fractal-like particle (agglomerate) growth ($D_{\text{f}} < 3$). The collision diameter, d_{c}, of agglomerates (equivalent to their diffusion diameter) formed by the coagulation of initially spherical (primary) particles of diameter d_{p} is[24]

$$d_{\text{c}} = d_{\text{p}} n_{\text{p}}^{1/D_f} \qquad (9)$$

where n_{p} is the number of primary particles per agglomerate. The agglomerate collision volume, $v_{\text{c}} = \pi d_{\text{c}}^3/6$, includes the volume of the constituent primary particles and the fluid between them. Agglomerate dynamics are calculated using eqs 2−7 as for $D_{\text{f}} = 3$ but with $d = d_{\text{c}}$ and an effective agglomerate density, ρ_{eff}. The latter is obtained from a mass/volume balance of a single agglomerate and eq 9

$$\rho_{\text{eff}} = \rho_{\text{f}} + (\rho_{\text{p}} - \rho_{\text{f}})(n_{\text{p}})^{1 - (3/D_{\text{f}})} \qquad (10)$$

where ρ_{f} is the fluid density. It should be noted that eq 4 might overestimate the friction coefficient of fractal particles.

A new agglomerate is formed when the collision volumes of two (or multiple) agglomerates (or periodic agglomerate images) touch or overlap. It contains all primary particles of the colliding

(19) Chandrasekhar, S. *Stochastic, Statistical, and Hydromagnetic Problems in Physics and Astronomy*; University of Chicago Press: Chicago, 1989.
(20) Ermak, D. L.; Buckholz, H. *J. Comput. Phys.* **1980**, *35*, 169−182.
(21) Kloeden, P. E.; Platen, E. *Numerical Solution of Stochastic Differential Equations*; Springer: Berlin, 1995.
(22) Heine, M. C.; de Vicente, J.; Klingenberg, D. J. *Phys. Fluids* **2006**, *18*, 023301.
(23) Smoluchowski, M. *Z. Phys. Chem.* **1917**, *92*, 129−168.
(24) Matsoukas, T.; Friedlander, S. K. *J. Colloid Interface Sci.* **1991**, *146*, 495−506.

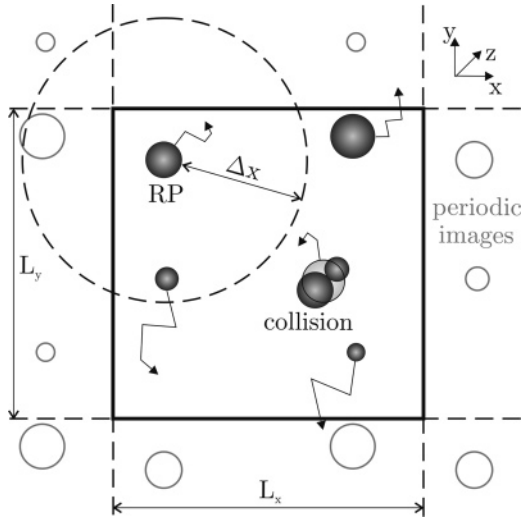

Figure 1. Schematic of Langevin dynamics simulations. Plane of three-dimensional fluid domain of size L_x, L_y, and L_z with periodic boundary conditions. Particles (or particle images) within Δx of the reference particle, RP, are stored in the particle neighbor list.

agglomerates, and its size is defined by eq 9. For $D_f < 3$, coagulation leads to an increase in the effective agglomerate volume fraction, ϕ_{eff},

$$\phi_{eff} = \frac{\pi \sum_{i=1}^{n} {d_{c,i}}^3}{6L_xL_yL_z} \geq \phi_s \tag{11}$$

but ϕ_s remains constant.

2.1.3. Particle Statistics and Growth Kinetics. The above Langevin dynamics (LD) simulations (Figure 1) result in detailed particle size distributions as a function of time.[15] Their geometric number-average, d_n, and volume-average, d_v, diameters are

$$\ln(d_n) = \frac{1}{n}\sum_{i=1}^{n} \ln(d_i) \text{ and}$$

$$\ln(d_v) = \sum_{i=1}^{n} \frac{v_i}{v_{tot}} \ln(d_i) \text{ with } v_{tot} = \sum_{i=1}^{n} v_i \tag{12}$$

The corresponding number-, σ_n, and volume-based, σ_v, geometric standard deviations are[25,26]

$$\ln(\sigma_n) = \left(\frac{1}{n-1}\sum_{i=1}^{n} \ln^2\left(\frac{d_i}{d_n}\right)\right)^{1/2} \text{ and}$$

$$\ln(\sigma_v) = \left(\sum_{i=1}^{n} \frac{v_i}{v_{tot}} \ln^2\left(\frac{d_i}{d_v}\right)\right)^{1/2} \tag{13}$$

Growth kinetics are characterized by the decay in particle number concentration. For particles undergoing coagulation and complete coalescence, having attained the self-preserving size distribution, this decay is[9]

$$\frac{dN}{dt}|_{dilute} = -\frac{1}{2}\beta_{dilute}N^2 \quad \text{with} \quad \beta_{dilute} = 1.0734\frac{8k_BT}{3\mu} \tag{14}$$

where $N = n/V_f$ is the particle number concentration and β_{dilute}, the overall collision frequency function, is 1.0734 times larger than that for monodisperse coagulation in the continuum regime[27] for dilute suspensions as described by the classic theory of coagulation.[23]

For any ϕ_s, knowing dN/dt from LD simulations, the corresponding overall collision frequency, β_{LD}, can be defined similar to eq 14:

$$\frac{dN}{dt}|_{LD} = -\frac{1}{2}\beta_{LD}N^2 \tag{15}$$

For particle suspensions having attained a self-preserving distribution (typically at $d_n/d_0 \geq 10$) at any ϕ_s, the enhancement of the overall collision frequency function, γ, of concentrated suspensions over dilute ones for a time period $\Delta t = t_2 - t_1$ is

$$\gamma = \frac{\beta_{LD}}{\beta_{dilute}} = \frac{2}{\beta_{dilute}}\frac{\frac{1}{N_2} - \frac{1}{N_1}}{t_2 - t_1} \tag{16}$$

where N_1 and N_2 are particle concentrations from LD simulations at t_1 and t_2.

The detailed collision frequency function $\beta_{i,j}$ from LD simulations can be determined, but a large number of collisions (e.g., >200) are needed to get accurate statistics. During data analysis, those statistics are improved by combining particles of similar size in sections[25]

$$1.2^{i-0.5} < \frac{d}{d_n} < 1.2^{i+0.5} \quad \text{for} \quad i = -i_{max}...i_{max} \tag{17}$$

where i is an integer and 1.2 is the geometric diameter spacing. The $\beta_{i,j}$ value between particles of sections i and j during time Δt is then given as[16]

$$\beta_{i,j} = \frac{P_{i,j}V_f}{n_in_j\Delta t} \quad \text{for} \quad i \neq j$$

$$\beta_{i,i} = \frac{2P_{i,i}V_f}{n_i(n_i-1)\Delta t} \quad \text{for} \quad i = j \tag{18}$$

where n_i and n_j are the number of particles assigned to sections i and j, respectively. $P_{i,j}$ describes the number of collisions between particles from sections i and j within time period Δt.

2.1.4. Numerical Computations. The particle trajectories (eqs 2 and 3) are calculated by the explicit Euler method.[15] The time step to resolve particle motion is chosen such that the root-mean-square particle displacement of particle i, Δx_i, is 2% of the particle diameter

$$\Delta t_i = \frac{{\Delta x_i}^2}{2D_i} = \frac{(0.02d_i)^2}{2D_i} \text{ with } D_i = \frac{k_BT}{f_i} \text{ for } i = 1...n \tag{19}$$

where D is the particle diffusivity. Δt_i decreases with decreasing particle size, so the integration time step is chosen dynamically according to the smallest particle ($d = d_{min}$) in the domain: $\Delta t = \min(\Delta t_i)$ for $i = 1...n$. The displacement of particles with $d > d_{min}$ is calculated using $z_i\Delta t \approx \Delta t_i$ (eqs 2 and 3), where z_i is a positive integer. The resulting displacement is then interpolated linearly during z_i integration time steps: $\Delta \mathbf{r}_i(\Delta t) = \Delta \mathbf{r}_i(k_i\Delta t)/z_i$. This approach of multiple time scales avoids numerical instabili-

(25) Hinds, W. C. *Aerosol Technology: Properties, Behavior, and Measurement of Airborne Particles*; Wiley: New York, 1999.

(26) Landgrebe, J. D.; Pratsinis, S. E. *J. Colloid Interface Sci.* **1990**, *139*, 63−86.

(27) Vemury, S.; Kusters, K. A.; Pratsinis, S. E. *J. Colloid Interface Sci.* **1994**, *165*, 53−59.

ties in eqs 2 and 3 that occur for $d_{max} \gg d_{min}$, where the displacement of the largest particle is essentially 0 at Δt.

The calculation domain is initially cubic with dimensions determined by the initial monodisperse particle size, particle number, and volume fraction:

$$L_x = L_y = L_z = d_0\left(\frac{\pi n_0}{6\phi_s}\right)^{1/3} \text{ at } t = 0 \qquad (20)$$

For $\phi_s < 25\%$, the initial particle positions are chosen randomly, avoiding overlapping particles. For $\phi_s \geq 25\%$, the above method fails, so particles are arranged into a cubic face-centered lattice. The structure is then disordered by randomly displacing particles with a Monte Carlo method.[28]

The computational speed is optimized for $\phi_s < 20\%$ by accounting only for collisions between a particle and particles in its vicinity through a so-called particle neighbor list.[28] For each particle, pointers to all particles (or image particles) closer than a predefined distance Δx are stored, and possible collisions between them are continuously checked (Figure 1). Once a collision takes place or the accumulated maximum particle displacement since the last calculation of the neighbor list is larger than 0.5 Δx, the neighbor list is updated.

2.2. Sectional Population Balance. A highly accurate sectional population balance with an adjustable geometric volume spacing of $2^{1/q}$ (e.g., $q = 4$) is used as a validation reference for the present LD simulations:[18]

$$\frac{dN_i}{dt} = \sum_{j=1}^{i-S(q)-1} \beta_{i-1,j} N_{i-1} N_j \frac{2^{(j-i+1)/q}}{2^{1/q}-1} + \sum_{k=2}^{q}\left(\sum_{j=i-S(q-k+2)-k+1}^{i-S(q-k+1)-k} \beta_{i-k,j} N_{i-k} N_j \frac{2^{(j-i+1)/q} - 1 + 2^{-(k-1)/q}}{2^{1/q}-1}\right) + \sum_{k=2}^{q}\left(\sum_{j=i-S(q-k+2)-k+2}^{i-S(q-k+1)-k+1} \beta_{i-k+1,j} N_{i-k+1} N_j \frac{-2^{(j-i)/q} + 2^{1/q} - 2^{-(k-1)/q}}{2^{1/q}-1}\right) + \frac{1}{2}\beta_{i-q,i-q} N_{i-q}^2 - \sum_{j=1}^{i-S(q)} \beta_{i,j} N_i N_j \frac{2^{(j-i)/q}}{2^{1/q}-1} - \sum_{j=i-S(q)+1}^{i_{max}} \beta_{i,j} N_i N_j \qquad (21)$$

with

$$S(a) = \sum_{b=1}^{a} b = \frac{a}{2}(a+1) \qquad (22)$$

For Brownian coagulation in the continuum regime $\beta_{i,j}$ is[9]

$$\beta_{i,j} = \frac{2k_B T}{3\mu}\left(\frac{1}{d_i} + \frac{1}{d_j}\right)(d_i + d_j) \qquad (23)$$

where d_i and d_j are the diameters of colliding particles from sections i and j, respectively.

3. Results and Discussion

All Langevin dynamics (LD) simulations are investigated in the continuum regime for particle growth by Brownian coagulation and complete coalescence in air at $T = 293$ K. Particles are initially monodisperse, $d_0 = 1$ μm in diameter, with a density of 1 g/cm^3. These conditions directly determine the self-preserving collision frequency from eq 14: $\beta_{dilute} = 6.4 \times 10^{-16}$ m^3/s.

3.1. Validation: Particle Diffusivity and Attainment of SPSD at Dilute Concentrations ($\phi_s \leq 0.1\%$). First, LD simulations are validated by monitoring the attainment of the classic values of particle diffusivity at any particle diameter in the continuum regime. Perfect agreement was obtained with textbook values of particle diffusivity. Figure 2a shows the evolution of the normalized particle number size distribution as obtained by LD simulations of initially $n_0 = 2000$ particles and dilute conditions ($\phi_s = 0.1\%$, $N_0 = 2 \times 10^{15}$ m^{-3}) at normalized average diameters of $d_n/d_0 = 1.2$ (circles), 2 (triangles), 15 (squares), and 150 (diamonds), corresponding to residence times of $t = 2$, 20, 8000, and 8×10^6 s, respectively. The distributions clearly converge to the classic dilute self-preserving size distribution (dotted line) of Brownian coagulation in the continuum regime[27,29] that is calculated by the sectional population balance (eqs 21−23) with $q = 4$. The large tail of these distributions calculated by LD simulations converges perfectly on the classic one, but the small tail takes a bit longer, as seen by Ulrich[30] and Landgrebe and Pratsinis[31] in the free molecular limit and Hidy in the continuum.[32]

Figure 2b shows the corresponding evolution of the number-based, σ_n (top), and volume-based, σ_v (bottom), geometric standard deviations for three different LD simulations (solid, broken, and dotted-broken lines). The initially monodisperse particle population ($\sigma_n = \sigma_v = 1.0$) broadens quickly during growth, reaching the self-preserving plateau[26] at $d_n/d_0 \approx 3$ and 1.5 for σ_n and σ_v, respectively. This indicates that an initially monodisperse suspension undergoing coagulation reaches its self-preserving distribution when its average diameter is 2 to 3 times its initial one regardless of particle concentration (data not shown), consistent with coagulation theory.[27,32] The time to reach this plateau is comparable to the theoretical time-lag of σ_n to attain self-preservation, τ_H[32] and τ_V[27],

$$\tau_H = \frac{3}{\pi D N_0 d} = \frac{25.76}{\beta_{dilute} N_0} = 21 \text{ s and}$$
$$\tau_V = \frac{6.34}{\pi D N_0 d_p} = \frac{54.443}{\beta_{dilute} N_0} = 45 \text{ s} \qquad (24)$$

that corresponds to $d_n/d_0 = 2.1$ (τ_H, vertical long broken line, Figure 2b) and 2.7 (τ_V, vertical double-dotted broken line). Once self-preservation is reached, σ_n and σ_v become 1.45 and 1.30, respectively, consistent with theory:[27] $\sigma_n = 1.445$ and $\sigma_v = 1.307$ (dotted lines). Fluctuations of σ_n and σ_v result from single-particle collisions that cause small variations in the size distributions. These fluctuations decrease for an increasing initial number of particles, but for $n_0 > 500$ particles, the statistics are sufficiently accurate so that the averaged properties of each LD simulation

(28) Allen, M. P.; Tildesley, D. J. *Computer Simulation of Liquids*; Clarendon Press: Oxford, U.K., 1987.

(29) Friedlander, S. K.; Wang, C. S. *J. Colloid Interface Sci.* **1966**, *22*, 126−132.

(30) Ulrich, G. D. *Combust. Sci. Technol.* **1971**, *4*, 47−57.

(31) Landgrebe, J. D.; Pratsinis, S. E. *Ind. Eng. Chem. Res.* **1989**, *28*, 1474−1481.

(32) Hidy, G. M. *J. Colloid Sci.* **1965**, *20*, 123−144.

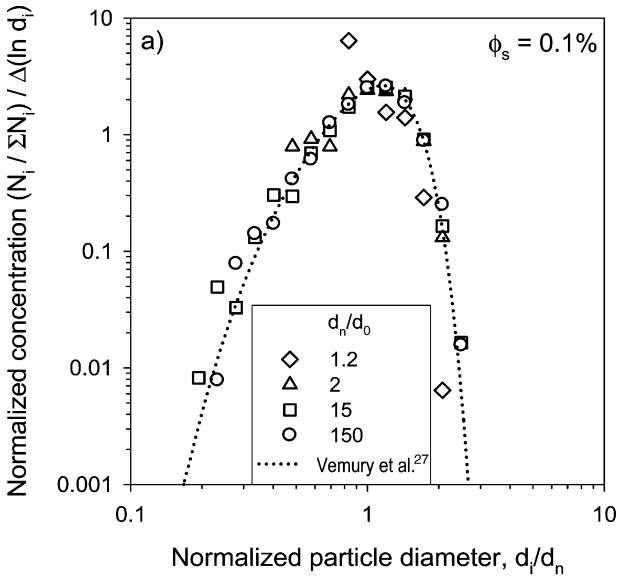

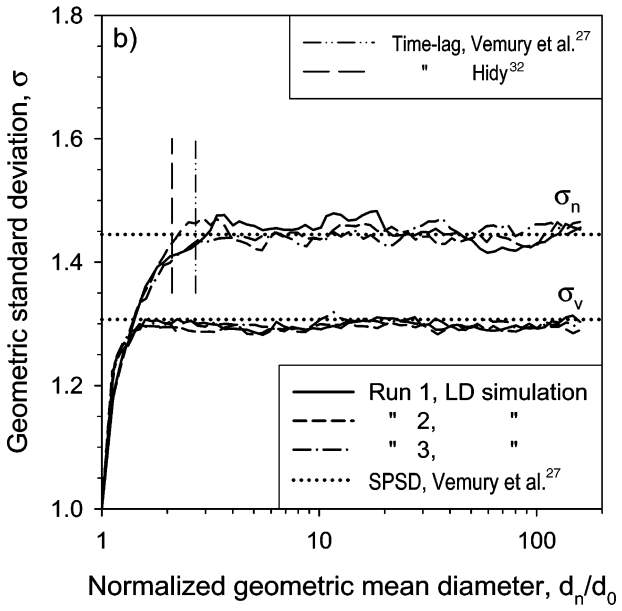

Figure 2. (a) Normalized particle number distributions at d_n/d_0 = 1.2 (◇), 2 (△), 15 (□), and 150 (○) corresponding to t = 2, 20, 8000, and 8 × 10^6 s, respectively. They were calculated by Langevin dynamics simulations with n_0 = 2000 particles under dilute conditions (ϕ_s = 0.1%) and approached the classic (dilute) self-preserving[27,29] distribution (···) at long enough times. (b) Evolution of the number-based, σ_n (top), and volume-based, σ_v (bottom), geometric standard deviations for three different LD simulations (solid, broken, and dotted-broken lines). All approach the dilute self-preserving σ_n and σ_v (dotted line) consistent with the theoretical time-lag for σ_n to attain self-preservation (vertical double-dotted broken line[27] and long broken line[32]). This means that coagulating suspensions become self-preserving when their average diameter d_n is 2 to 3 times the initial d_0.

converge to the same solution. Here, n_0 = 2000 is also used to accurately represent distributions broader than the self-preserving limit.

The exact self-preserving size distribution (SPSD) can be obtained by averaging over several distributions after a suspension has attained ($d_n/d_0 \geq 10$) its self-preservation (Figure 2b). Alternatively, n_0 could be increased, but this leads to an exponential increase in computational cost. Figure 3 shows such an average of 90 distributions (symbols) for ϕ_s = 0.1% and n_0 = 2000 that is in excellent agreement with the SPSD[27] in the continuum regime (dotted line).

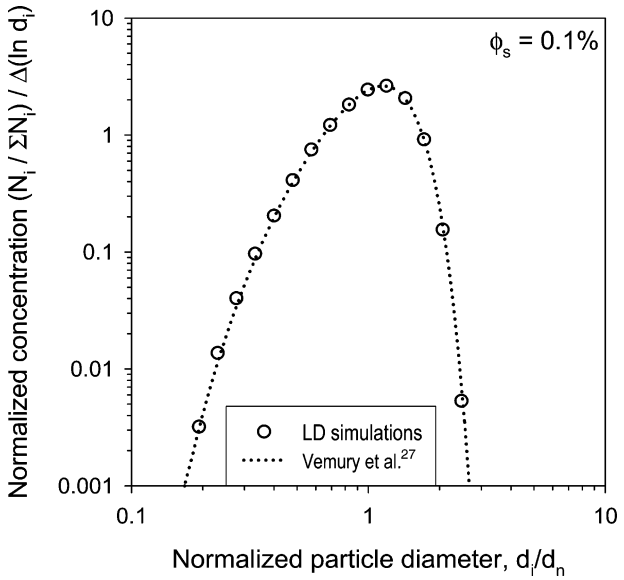

Figure 3. Self-preserving size distribution obtained from Langevin dynamics simulations (○) by averaging 90 distributions after self-preservation is attained (d_n/d_0 > 10) for ϕ_s = 0.1% and n_0 = 2000. It is in excellent agreement with the population balance simulations of Vemury et al.[27] in the continuum regime (···).

3.2. Concentrated Particle Dynamics. Figure 4a shows the effect of particle volume fraction on the SPSD from LD simulations at ϕ_s = 1 (circles), 10 (squares), 20 (diamonds), and 30% (triangles) following the procedure of Figure 3. At ϕ_s = 1%, the SPSD is almost identical to the classic SPSD under dilute conditions (Figure 2a, dotted line). For ϕ_s > 1%, however, the SPSD broadens continuously for increasing ϕ_s, and the distribution becomes less symmetric. This becomes more pronounced as ϕ_s increases from 1 to 30%.

Figure 4b shows the evolution of the number-based, σ_n (top), and volume-based, σ_v (bottom), geometric standard deviations for three different runs (as in Figure 2b) but at ϕ_s = 20%. As with coagulation at dilute concentrations, both σ values reach a plateau, regardless of initial conditions, indicating the attainment of self-preserving distributions.[33] σ_v quickly reaches its plateau at about $d_n/d_0 \approx 1.8$ as under dilute conditions (ϕ_s = 0.1%, Figure 2b), but it is slightly larger (σ_v = 1.32) than that of the classic dilute SPSD (σ_v = 1.307). σ_n levels off at 1.68, so it is significantly larger than 1.445 under dilute conditions (Figure 2b). Additionally, the time-lag to attain self-preservation for σ_n (eq 24) increases and corresponds to $d_n/d_0 \approx 6$ at ϕ_s = 20% compared to 2.7 in the dilute limit (Figure 3b, vertical double-dotted broken line).

Figure 5 shows the asymptotic σ_n and σ_v of the SPSD as function of ϕ_s. Below ϕ_s = 1%, LD calculations match the geometric standard deviations: σ_n = 1.445 and σ_v = 1.307 in classic coagulation theory.[27] For larger ϕ_s, however, σ_n increases to 1.52, 1.68, and 2.35 at ϕ_s = 10, 20, and 30%. σ_v is almost constant up to about ϕ_s = 10% and then increases to a lesser extent than σ_n, reaching 1.32 and 1.39 at ϕ_s = 20 and 30%, respectively. In general, σ_n is larger than σ_v, resulting from the nonsymmetric SPSD having a narrower tail for large rather than for small particles. The above results show that in the continuum regime SPSDs develop at all ϕ_s values up to 35% and strongly depend on ϕ_s, in contrast to classic coagulation theory.

3.3. Overall Coagulation Rate at High Concentration. Figure 6 shows the enhanced overall collision frequency function (β_{LD}, normalized with β_{dilute}), $\gamma = \beta_{LD}/\beta_{dilute}$ (eq 16), as a function of

(33) Ernst, F. O.; Pratsinis, S. E. *J. Aerosol. Sci.* **2006**, *37*, 123−142.

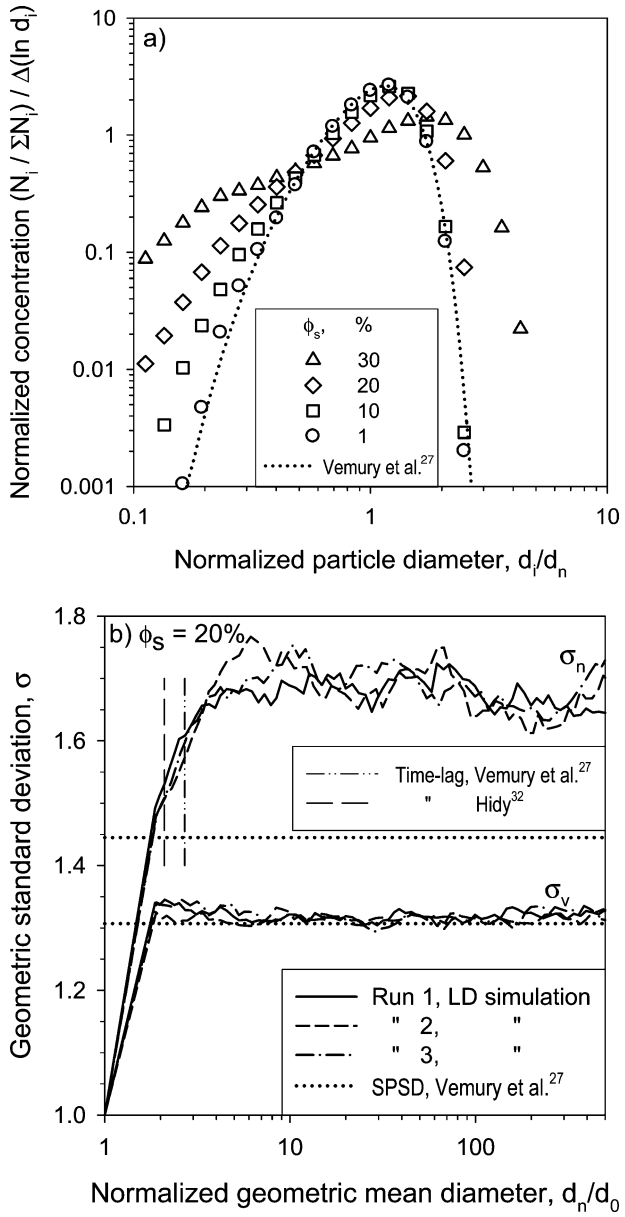

Figure 4. (a) Self-preserving size distributions by Langevin dynamics simulations at $\phi_s = 1$ (○), 10 (□), 20 (◊), and 30% (△) that remain invariant with time once self-preservation is attained. (b) Evolution of the number-based, σ_n (top), and volume-based, σ_v (bottom), geometric standard deviations for three different Langevin dynamics simulations (solid, broken, and dotted-broken lines) as in Figure 2b but at $\phi_s = 20\%$. Self-preservation is attained when the average particle diameter d_n is 5−8 times the initial one, d_0.

ϕ_s (circles) after SPSD has been attained. γ is always above unity, so coagulation kinetics at high ϕ_s are faster than those predicted by eq 14 for the coagulation of dilute suspensions. For the lowest particle concentration investigated here ($\phi_s = 0.01\%$), $\gamma = 0.99$ was found to be in agreement with the classic SPSD theory ($\gamma_{dilute} = 1.0$) for dilute particle concentrations (dotted line, eq 14). At $\phi_s = 0.1$ and 1%, γ is 1.08 and 1.44, respectively, meaning that the overall coagulation rate is 8 and 44% faster than that given by classic Smoluchowski theory (eq 14). In the ϕ_s range of 0.01 to 1%, a transition from dilute to concentrated particle dynamics takes place, where classic coagulation theory is no longer valid and underpredicts β. At $\phi_s = 3\%$, the coagulation kinetics are nearly twice as fast ($\gamma = 1.94$) and increase further to $\gamma = 3.6$ and 8.7 at $\phi_s = 10$ and 20%, respectively. Neglecting the effect of high concentrations, especially for $\phi_s > 1\%$, results

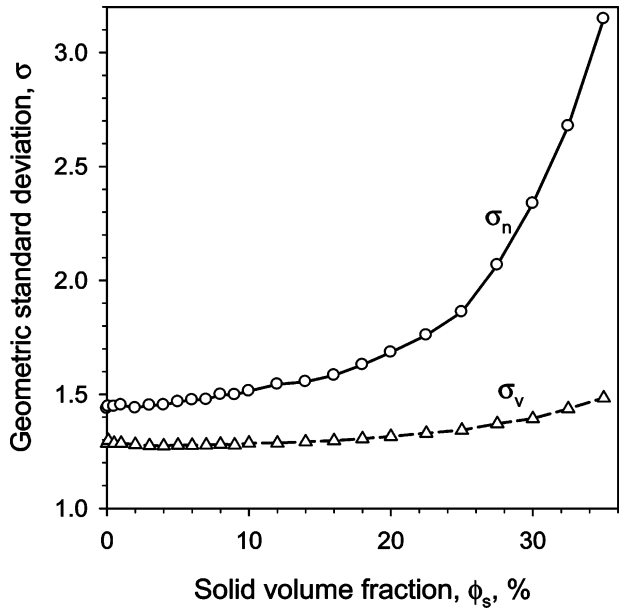

Figure 5. Self-preserving number-based, σ_n (○), and volume-based, σ_v (△), geometric standard deviations as a function of the solid volume fraction, ϕ_s. Because the broadening of the SPSD with increasing ϕ_s is more pronounced in the small tail (Figure 4a), σ_n is more sensitive to ϕ_s than σ_v.

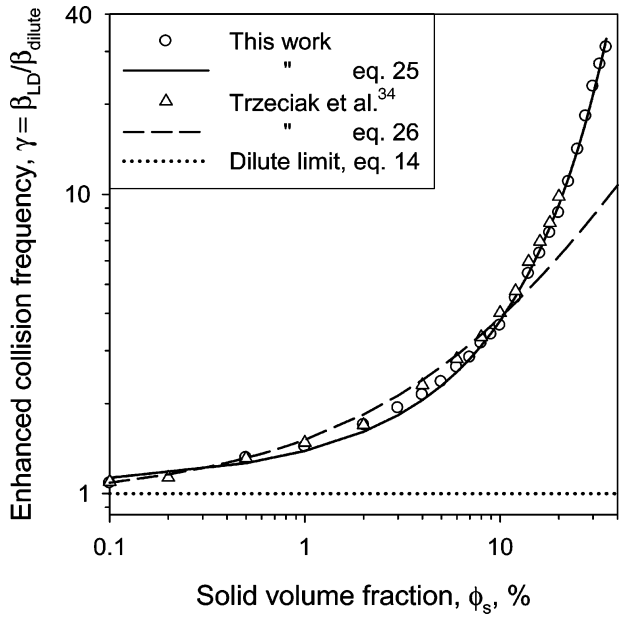

Figure 6. Enhanced overall collision frequency function from LD simulations, $\gamma = \beta_{LD}/\beta_{dilute}$ (eq 16), as function of ϕ_s (○), along with the corresponding regression (solid line, eq 25). The monodisperse LD simulations of Trzeciak et al.[34] (△) along with their regression (broken line, eq 26) are shown also.

in a significant underestimation of the coagulation kinetics that are more than 30 times faster than those from classic Smoluchowski theory at $\phi_s = 35\%$ ($\gamma \approx 31$).

The present work agrees well with the LD simulations of Trzeciak et al.[34] (Figure 6, triangles) despite differences in the model assumptions. In contrast to the present work, they[34] assume monodisperse particles of constant diameter at all times. To preserve the particle number and volume fraction upon collision, one of the colliding particles is removed and redistributed into

(34) Trzeciak, T. M.; Podgórski, A.; Marijnissen, J. C. M. In *5th World Congress on Particle Technology*, Orlando, FL, 2006; p 202d.

the fluid domain of constant dimensions. This redistribution is done by an algorithm that maintains the particle pair correlation function during redistribution. Effects of particle growth, such as the polydispersity of the resulting distribution or momentum transfer upon collision, had not been accounted for.[34]

Figure 6 also shows a best-fit regression line (solid line) of the present LD data (circles) describing γ up to $\phi_s = 35\%$ by

$$\gamma = \frac{\beta_{LD}}{\beta_{dilute}} = 1 + \frac{2.5}{1-\phi}(-\log \phi)^{-2.7} \qquad (25)$$

where $\phi = \phi_s$ for full particle coalescence and $\phi = \phi_{eff}$ for fractal particle growth. This equation reduces to the classic Smoluchowski result for dilute suspensions $(-\log \phi)^{-2.7} \ll 1$, so the second right-hand side term of eq 25 is essentially zero and $\beta_{LD} = \beta_{dilute}$. For high particle concentrations (ϕ close to unity[35]), $2.5/(1-\phi)$ becomes large, and eq 25 describes enhanced particle growth that becomes infinite (indicating gelation[33]) for the highest possible polydisperse packing density of near unity.[35] Equation 25 can be used to replace $\beta_{i,j}$ with $\gamma\beta_{i,j}$ to correctly describe the overall decay in total particle number concentration for concentrated suspensions but not the correct SPSD and polydispersity (Figure 4a,b). Trzeciak et al.[34] also proposed a regression line (broken line) for the overall coagulation rate at high concentration:

$$\gamma = \frac{\beta_{dilute}}{1.0734}(1 + 12\phi + \sqrt{24\phi(1+6\phi)}) \qquad (26)$$

For dilute suspensions ($\phi \ll 0.1\%$), eq 26 converges to the classic monodisperse collision frequency ($\gamma = 1/1.0734$) and agrees well with ours and their LD simulations for $\phi \leq 10\%$.

3.4. Collision Frequency Function. Figures 4−6 show that high particle concentration leads to enhanced coagulation kinetics and wider SPSDs. This results from changes in the collision frequency function that can no longer be described only as a function of particle collision area and diffusivity according to classic theory (eq 23). To obtain a better understanding of high concentration effects on coagulation, the collision frequency function is calculated directly from the LD collision statistics.

3.4.1. Dilute Concentrations ($\phi_s \leq 0.1\%$). Figure 7 shows the normalized collision frequency function under dilute conditions ($\phi_s = 0.1\%$) as a function of the relative particle diameter, d_j/d_i. $\beta_{i,j}/\beta_{dilute}$ for the dilute limit (dotted line) shows the classic result of eq 23. It has a minimum for equally sized particles at $\beta_{i,j}/\beta_{dilute} = 1/1.0734 = 0.9316$ and faster collision frequencies for differently sized particles. The latter results from the fact that smaller particles diffuse faster but have a smaller collision area compared to larger ones, so differently sized particles have higher collision probabilities because one particle diffuses quickly and the other provides a large collision area.[9]

Because LD simulations predict faster coagulation kinetics than eq 23 for $\phi_s > 0.01\%$, $\beta_{i,j}/\beta_{LD}$ (Figure 6, eq 15) is used for better comparison. $\beta_{i,j}/\beta_{LD}$ depends only on the size ratio d_i/d_j and agrees perfectly with $\beta_{i,j}$ for the classic dilute limit. The LD-calculated $\beta_{i,j}$ values are shown for $n_0 = 2000$ at various $d_i/d_n = 0.5$ (diamonds), 1 (triangles), and 2 (circles) that correspond to particles from the smaller end, the center, and the larger end of the SPSD (Figure 2a), respectively. Each data point represents 200 to 10 000 collisions in the LD simulations to ensure sufficient statistics. For example, particles with $d_i/d_n =$ 2 mainly collide with smaller particles, so the corresponding line is resolved best for $d_j/d_i < 1$.

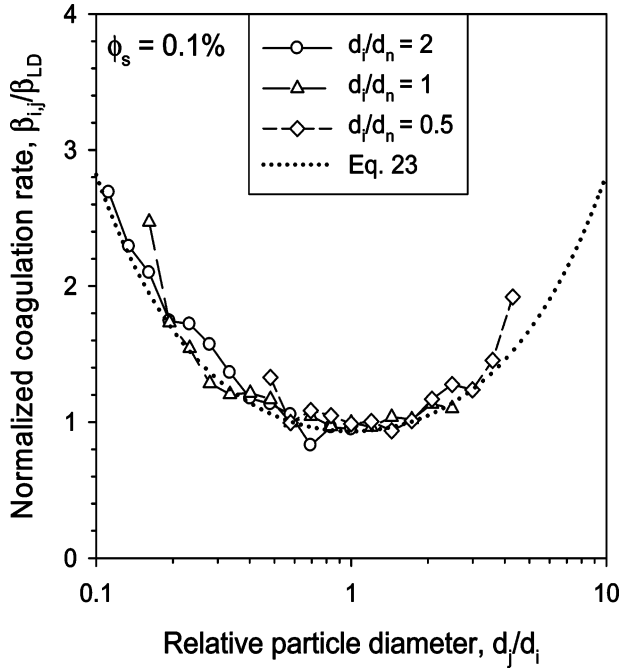

Figure 7. Normalized collision frequency function from LD simulations, $\beta_{i,j}/\beta_{LD}$, at dilute conditions ($\phi_s = 0.1\%$) and $d_i/d_n = 0.5$ (◇), 1 (△), and 2 (○) are in excellent agreement with the classic dilute limit (···, eq 23).

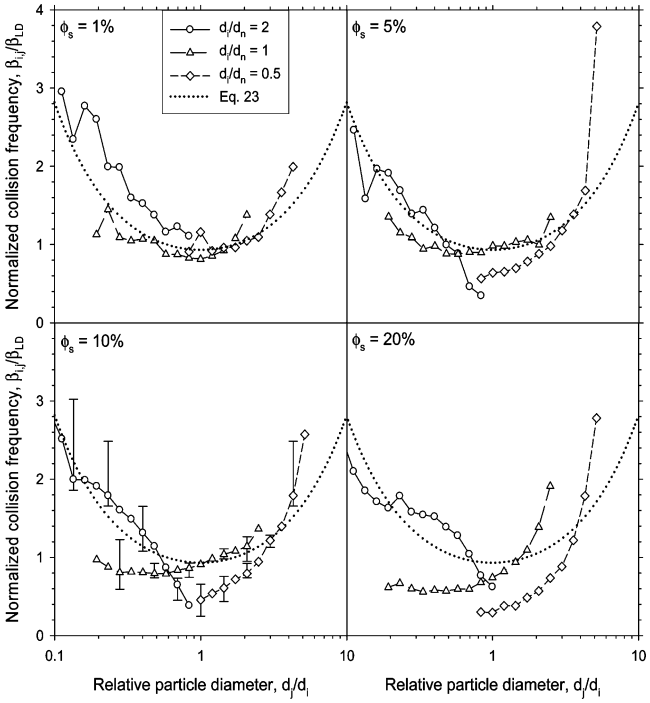

Figure 8. Normalized collision frequency functions from LD simulations, $\beta_{i,j}/\beta_{LD}$, at $\phi_s = 1$, 5, 10, and 20% and $d_i/d_n = 0.5$ (◇), 1 (△), and 2 (○) compared to the classic dilute limit (···, eq 23). The collision frequency function at increasing ϕ_s scatters more from its dilute counterpart even though they are broadly consistent with each other.

3.4.2. High Concentrations ($\phi_s > 0.1\%$). Figure 8 shows the normalized collision frequency function as in Figure 7 but for increasing particle concentrations of $\phi_s =$ (a) 1, (b) 5, (c) 10, and (d) 20%. At $\phi_s = 1\%$, $\beta_{i,j}$ generally follows the results for the dilute limit (dotted lines) but predicts slightly increased collision

(35) Herrmann, H. J.; Baram, R. M.; Wackenhut, M. *Braz. J. Phys.* **2003**, *33*, 591−593.

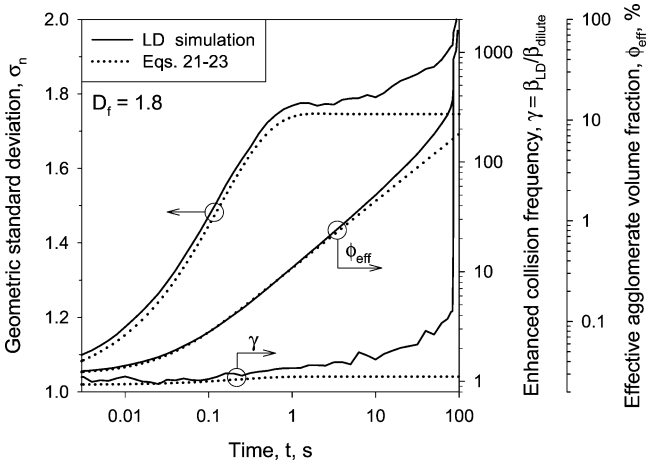

Figure 9. Fractal-like ($D_f = 1.8$) agglomerate dynamics at high (industrial-like) concentrations. Evolution of the number-based geometric standard deviation, σ_n (based on agglomerate d_c), enhanced collision frequency, $\gamma = \beta_{LD}/\beta_{dilute}$, and effective agglomerate volume fraction, ϕ_{eff}, as function of time. The average of 10 LD simulations (−) is shown together with classic sectional simulations (eq 21−23, $q = 4$, ···). Agglomerates attain a self-preserving distribution (SPSD) only temporarily (until about 10 s: $\sigma_n \approx 1.8$). They deviate from the SPSD as their effective volume fraction increases, approaching gelation.

frequencies between smaller and larger particles for $d_i/d_n = 2$ (circles). At $\phi_s = 5$, 10, and 20%, the results for $d_i/d_n = 0.5$ (diamonds), 1 (triangles), and 2 (circles) increasingly diverge, so $\beta_{i,j}$ can no longer be described only by eq 23. The increase in $\beta_{i,j}$ for increasing particle size ratio d_j/d_i at $d_i/d_n = 0.5$ and 1 is steeper than for dilute conditions (Figure 7), and the slope increases with increasing ϕ_s. This shows that steric effects such as caging or shielding of large particles by smaller ones at increasingly high ϕ_s enhance the collisions of smaller particles with larger ones. In contrast, larger particles with $d_i/d_n = 2$ have reduced collision probabilities with particles of similar size (circles, d_j/d_i close to unity). This might result from the high number concentration of smaller particles (Figure 4a) that may surround larger particles so that the collision pathway between two large particles is hindered. This shows that in concentrated suspensions $\beta_{i,j}$ cannot be predicted without information about ϕ_s and d_n, in contrast to dilute suspensions that are accurately described by classic coagulation theory.

It should be noted that the results of Figure 8 could also be obtained by omitting the effect of inertia (in eq 1, the left-hand side equals zero) in the LD calculations, so high concentration dynamics are not caused by ballistic effects due to small stopping distances between particles but result primarily from steric hindrance.

3.5. Fractal Agglomerate Growth. The growth of silica agglomerates with a constant fractal dimension of $D_f = 1.8$ is investigated during Brownian coagulation in the continuum at room temperature in air neglecting rotation at these rather high D_f values.[36] Agglomerates have initially monodisperse collision diameters of $d_{c,0} = 220$ nm and consist of $d_p = 21$ nm (SSA = 130 m^2/g) primary particles. The initial agglomerate concentration is $N_0 = 5.4 \times 10^{16}$ m^{-3} corresponding to $\phi_{eff} = 0.03\%$, consistent with the onset of (soft) agglomerate formation during fumed silica synthesis by the hydrolysis of $SiCl_4$ at industrial conditions.[13]

Figure 9 shows the evolution of σ_n (calculated from eq 13 with $d = d_c$), $\gamma = \beta_{LD}/\beta_{dilute}$, and ϕ_{eff} as function of time for LD (solid lines) and classic sectional simulations with $q = 4$ (eqs 21−23, dotted lines). The good agreement of both simulations under dilute conditions ($t < 1$ s, $\phi_{eff} < 0.4\%$) validates the LD simulations for the growth of fractal-like agglomerates (eqs 1−3 and 9−10).

Both simulations predict a continuous increase in ϕ_{eff} during growth as ρ_{eff} decreases with increasing agglomerate size (eq 10). For $t > 1$ s, the LD simulations result in enhanced collision frequencies ($\gamma > 1$) until $t = 95$ s, where σ_n and γ increase rapidly, indicating gelation[33] in the absence of agglomerate restructuring or fragmentation. σ_n increases with time as the agglomerate size distribution develops ($t < 1$ s) and for the sectional simulations reaches an SPSD with $\sigma_n = 1.746$ for $D_f = 1.8$ ($\sigma_n = 1.397$ on the basis of the coalesced agglomerate diameter, consistent with Vemury and Pratsinis[37]). For $t < 1$ s, LD simulations show a similar evolution but predict slightly larger σ_n values than do sectional simulations. However, no SPSD is attained, even at long residence times ($t > 1$ s), but the distribution broadens continuously as ϕ_{eff} increases. In general, the effect of ϕ_{eff} on fractal agglomerate growth is comparable to that of ϕ_s for $D_f = 3$ (Figure 5). At short times ($t < 0.1$ s), LD simulations result in $\gamma \approx 1$ as predicted by classic theory, but for $t > 0.1$ s ($\phi_{eff} > 0.08\%$), coagulation accelerates (Figure 9) and doubles at $t = 20$ s ($\phi_{eff} = 3\%$) and is consistent to $\phi_s = 3\%$ and $D_f = 3$ (Figure 6).

γ (Figure 9) accelerates further and becomes about 100 times faster than that predicted by classic coagulation theory (eq 14 and 23) when the suspension approaches gelation ($t > 80$ s). This is consistent with light-scattering data during the aerogelation of fractal soot clusters where coagulation kinetics were more than 2 orders of magnitude faster than expected from classical theory.[17] More compact, fractal-like agglomerates exhibit the same qualitative behavior as in Figure 9; for example, the onset of gelation takes place at $t = 10^6$ s for $D_f = 2.2$.

4. Conclusions

The effect of particle volume fraction on particle growth by Brownian coagulation and complete coalescence in the continuum regime is investigated from first principles by calculating particle motion and collisions with the Langevin differential equation. Self-preserving particle size distributions (SPSD) are obtained at all investigated particle volume fractions, from $\phi_s = 0.01$−35%, but the classic self-preserving theory is valid only for $\phi_s < 1\%$. For increasing ϕ_s, the SPSD broadens as its number-based geometric standard deviation becomes 1.52, 1.68, and 2.35 at $\phi_s = 10$, 20, and 30%, respectively, compared to 1.445 for classic Smoluchowski coagulation. The SPSD is attained when the average particle diameter is 5−10 times its initial value at high concentration in contrast to 2 to 3 times its initial value at classic, dilute concentration.

Changes in the SPSD are accompanied by a significant increase in the rate of coagulation for ϕ_s above 0.01%. The overall collision frequency is 3.6, 8.7, and 31 times faster than the frequency from classic theory at $\phi_s = 10$, 20, and 35%, respectively. Changes in SPSD and coagulation kinetics result from changes in the detailed collision frequency function that becomes a complex function of the particle size ratio, particle volume fraction, and average particle size. Steric effects from interfering small particles seem to reduce the collision frequency between large particles.

High concentration significantly increases the coagulation rate of fractal-like particles (agglomerates), consistent with experimental observations. For agglomerates, even initially low particle volume fractions ($\phi_s < 0.01\%$) can become effectively large

(36) Gradon, L. Personal communication, 2007.

(37) Vemury, S.; Pratsinis, S. E. *J. Aerosol. Sci.* **1995**, *26*, 175−185.

(ϕ_{eff} > 10%) because growing agglomerates occupy far more volume than their equivalent solid mass. As a result, agglomerates may experience a transition from dilute to highly concentrated coagulation dynamics that can lead to gelation. For fractal-like agglomerates with constant D_f, only a temporary SPSD can be reached at concentrated conditions (ϕ_{eff} > 0.1%) as coagulation kinetics accelerate continuously until gelation.

Acknowledgment. Financial support from the Swiss National Science Foundation (SNF) (200020-107947/1) is gratefully acknowledged.

Notation

a	place holder
d	particle diameter (m)
D	particle diffusivity ($m^2\ s^{-1}$)
f	friction coefficient (kg s^{-1})
F	general function
G	mean square value of **V**
H	average scalar product of **V** and **R**
i	index for particle or section
I	mean square value of **R**
j	index for particle or section
k	index for section
k_B	Boltzmann constant (J K^{-1})
L	length of the domain (m)
m	particle mass (kg)
n	number of particles in the fluid domain volume
n_p	number of primary particles per agglomerate
N	particle number concentration (m^{-3})
P	collisions between particles
q	spacing exponent
r	particle position vector (m)
R	stochastic component of particle position vector (m)
S	function
t	time (s)
T	temperature (K)
v	particle velocity vector (m s^{-1})
V	stochastic component of particle velocity (m s^{-1})
V_f	fluid domain volume (m^3)
w	fluid velocity vector (m s^{-1})
x	distance (m)
Y	Gaussian distributed random number
z	positive integer

Greek Symbols

α	mass related friction coefficient (s^{-1})
β	particle collision frequency function ($m^3\ s^{-1}$)
ϕ	particle volume fraction
γ	enhanced collision frequency function
μ	fluid viscosity (kg $m^{-1}\ s^{-1}$)
ρ	density (kg m^{-3})
σ	geometric standard deviation
τ	time lag to attain self-preservation (s)

Indices

0	initial ($t = 0$)
c	collision
dilute	dilute conditions
eff	effective
ext	external
f	fluid
LD	Langevin dynamics
max	maximum
min	minimum
n	number
p	primary particle
s	solid
tot	total
v	volume
x, y, z	spatial directions

LA7012599